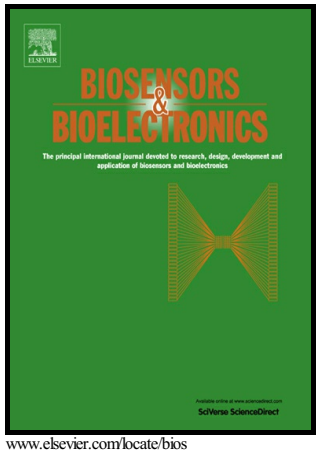

www.elsevier.com/locate/bios

Modelling of magnetoimpedance response of thin film sensitive element in the presence of ferrogel: Next step toward development of biosensor for in-tissue embedded magnetic nanoparticles detection

N.A. Buznikov, A.P. Safronov, I. Orue, E.V. Golubeva, V.N. Lepalovskij, A.V. Svalov, A.A. Chlenova, G.V. Kurlyandskaya

PII: S0956-5663(18)30464-0
DOI: https://doi.org/10.1016/j.bios.2018.06.032
Reference: BIOS10552

To appear in: *Biosensors and Bioelectronic*

Received date: 29 April 2018
Revised date: 29 May 2018
Accepted date: 19 June 2018

Cite this article as: N.A. Buznikov, A.P. Safronov, I. Orue, E.V. Golubeva, V.N. Lepalovskij, A.V. Svalov, A.A. Chlenova and G.V. Kurlyandskaya, Modelling of magnetoimpedance response of thin film sensitive element in the presence of ferrogel: Next step toward development of biosensor for in-tissue embedded magnetic nanoparticles detection, *Biosensors and Bioelectronic,* https://doi.org/10.1016/j.bios.2018.06.032

Modelling of magnetoimpedance response of thin film sensitive element in the presence of ferrogel: Next step toward development of biosensor for in-tissue embedded magnetic nanoparticles detection

N.A. Buznikov[1], A.P. Safronov[2,3], I. Orue[4], E.V. Golubeva[2], V.N. Lepalovskij[2], A.V. Svalov[3], A.A. Chlenova[2], G.V. Kurlyandskaya[2,5*]

[1]Scientific and Research Institute of Natural Gases and Gas Technologies—Gazprom VNIIGAZ, Razvilka, Leninsky District, Moscow Region 142717, Russia
[2]Institute of Natural Sciences and Mathematics, Ural Federal University, Ekaterinburg 620002, Russia
[3]Institute of Electrophysics, Ural Division RAS, Ekaterinburg 620016, Russia
[4]Advanced Research Facilities (SGIKER), Universidad del País Vasco UPV-EHU, 48080 Bilbao, Spain
[5]Department of de Electricity and Electronics, University of the Basque Country UPV-EHU, Bilbao 48080, Spain

[*]Corresponding author. Tel.: +34-9460-13237; fax: +34-9460-13071. galina@we.lc.ehu.es

Abstract

In-tissue embedded magnetic nanoparticle (MNPs) detection is one of the most interesting cases for cancer research. In order to understand the origin, the limits and the way of improvement of magnetic biosensor sensitivity for the detection of 3D mezoscopic distributions of MNPs, we have developed a magnetoimpedance biosensor prototype with a [Cu (3 nm)/FeNi(100 nm)]$_5$/Cu(500 nm)/[FeNi(100 nm)/Cu(3 nm)]$_5$ rectangular sensitive element. Magnetoimpedance (MI) responses were measured with and without polyacrylamide ferrogel layer mimicking natural tissue in order to evaluate stray fields of embedded MNPs of γ-Fe_2O_3 iron oxide. A model for MI response based on a solution of Maxwell equations with Landau-Lifshitz equation was developed in order to understand the origin of the prototype sensitivity which reached 1.3 % of $\Delta Z/Z$ per 1 % of MNPs concentration by weight. To make this promising technique useful for magnetically labeled tissue detection, a synthesis of composite gels with MNPs agglomerates compactly located inside pure gel and their MI testing are still necessary.

Keywords: Magnetic biosensor; Magnetic nanoparticles detection; Ferrogels; Biomimetic materials; Magnetoimpedance; Magnetic multilayers

1. Introduction

Magnetic biosensing for biomedical engineering is a rapidly growing area of multidisciplinary research focused on the development of new techniques for the evaluation of properties of biological objects. It is the magnetic properties of biological objects that attract special attention [Glazer, 1999; Baselt, 1998; Shanmugam, 2009; Grossman, 2012]. Nanomaterials and magnetic nanoparticles have been widely studied for their biomedical application [Chen, 2018; Rusakov, V., 2018]. Significant efforts have been made for the development of a magnetic field sensors adapted for biosensing [Ferreira, 2002; Miller, 2002; Besse, 2002]. Modern measuring devices allow a quantified evaluation of small changes in the magnetic susceptibility, in the effective magnetic anisotropy in the living system, or in magnetic field values created by the extracellular electric currents. However, there is a need to improve

their sensitivity and specificity and to further develop their design up to miniaturized analytical systems [Devkota, 2014; Wang, 2017].

We define a magnetic biosensor as a compact analytical device incorporating a biological or biologically derived sensitive element, integrated in the physicochemical transducer employing a magnetic field and magnetic materials [Kurlyandskaya, 2017]. Different physical phenomena were shown to have the capacity to support the development of magnetic biosensor prototypes for both label free [Ong, 2001; Kurlyandskaya, 2006, Huang, 2009; Lopez, 2018] and magnetic label detection processes [Graham, 2003; Blanc-Beguin 2009; Garcia-Arribas 2011; Yang, 2010].

One of the most important parameters insuring the successful functionality of a magnetic biosensor is the sensitivity of the physical sensitive element to the variations of the external magnetic field. In the case of magnetic label detection, the magnetic field sensor evaluates the disturbance of the external magnetic field using the stray fields of magnetic labels present in the test solution [Baselt, 1998; Graham, 2003; Kurlyandskaya, 2005]. This is why, the giant magnetoimpedance effect (MI) or large variation of the total impedance of ferromagnetic conductor under application of the external magnetic field, have attracted special attention [Makhotkin 1991; Uchiyama, 2012].

The superparamagnetic labels that are part of the molecular recognition-based sandwiches are situated at certain small distances in classic magnetic biosensors for the evaluation of the concentration of the biocomponent of interest in the test solution [Baselt, 1998; Wang, 2017]. In order to measure the concentration of magnetic nanoparticles (MNPs) in the continuous flow in the microfluidic system, after their intracellular up-take, or in-tissue embedded MNPs, a much stronger sensitivity demand should be established. The physical origin of this demand is due to the fact that uniformly magnetized superparamagnetic sphere stray fields can be approximated by the magnetic dipole generating the stray fields inversely proportional to the cube of the distance between the dipole centre and the point of the measurement [Landau, 1975].

In the simplest magnetic biosensor, the operational distances between magnetic labels and the surface of the magnetic sensitive element are all the same and they are very small (of the order of 1 nm) [Wong, 1999] and their interpretation is simple. In more complex cases, especially interesting for cancer research (in-tissue embedded MNPs), the distances between MNPs and the surface of the sensitive element are different and special modeling and signal processing are necessary. In this case, the sensitivity of the magnetic element with respect to the external magnetic field becomes a crucial parameter. Recently, there were efficient demonstrations of the capability of GMI sensitive elements based either on thin film structures or amorphous ribbons to measure the concentration dependences of the MNPs embedded in a ferrogel matrix successfully mimicking many functions of the natural tissue [Kurlyandskaya, 2015; Safronov, 2018]. At the same time, a clear understanding of the origin, limits and way of improvement of magnetic biosensor sensitivity for detection of 3D mezoscopic distributions of MNPs is still absent.

We therefore propose an experimental study supported by an electrodynamic model developed for ferrogel detection by multilayered structure magnetoimpedance-based biosensor prototype. To mimic natural tissue with embedded MNPs we used chemically crosslinked hydrogels filled with maghemite Fe_2O_3 MNPs. Giant magnetoimpedance sensor prototype responses were measured with and without covering by a gel or ferrogel layer. The corresponding model for MI was proposed in order to understand the origin of prototype sensitivity.

2. Experimental

2.1. Fabrication of tissue mimicking gels and ferrogels

For the present study, weekly aggregated magnetic nanoparticles were synthesized by the electrophysical technique of laser target evaporation of an iron oxide target [Safronov, 2013]. Pulsed Ytterbium laser evaporation (wavelength 1.07 μm) was done with a pulse frequency of 4.85 KHz, pulse duration of 60 μs and an average output power of 262 W. The condensation of MNPs from vapour took place in a continuous flow of argon at 5 L/min flow rate. Nanoparticles obtained by electrophysical techniques are characterized by a high surface activity causing the tendency to form aggregates in suspensions. Actually, the inevitable aggregation of nanoparticles during re-dispersion in suspension is one of the main problems in air-dry powder processing [Zhang, 2008; Hwang, 2008]. Usually, even methods of ultrasonic dispersion or high shear mixing do not guarantee complete de-aggregation [Chung, 2009; Pacek, 2007]. In the case of iron oxide dry powders, magnetic dipole-dipole interactions also contribute to the interaction between MNPs apart from the interactions driven by surface forces. Therefore, we used some of the results obtained in our special studies on the factors of the colloidal stability of iron oxide MNPs in water suspensions [Beketov 2012] in order to obtain de-aggregated nanoparticles in the state of magnetic nanofluid

Prior to the synthesis of ferrogels, an electrostatically stabilized ferrofluid based on iron oxide MNPs in 2.3 wt.% concentration was prepared in a 5 mM sodium citrate solution in distilled water by ultrasound treatment with permanent cooling using a Cole-Parmer CPX-750 processor (Cole-Parmer Instruments Corp. Vernon Hills, IL, USA). Polyacrylamide (PAAm) ferrogels were synthesized by the free-radical polymerization of acrylamide (AppliChem, Darmstadt, Germany) in 2.7 M aqueous solution with N,N'-methylene-diacrylamide (Merck Schuchardt, Hohenbrunn, Germany) as a cross-linker, which was taken in 1:50 molar ratio to the monomer. Polymerization was performed at 25 °C with ammonium persulfate in 3 mM concentration as an initiator and N,N,N’,N’-tetramethylethylene diamine (TEMED) (SigmaAldrich Inc. St. Louis MO, USA) in 6 mM concentration as a catalyst.

Before the GMI experiments, the gels and ferrogels were washed in distilled water for two weeks with daily water renewal until the equilibrium water uptake was achieved. The obtained series of ferrogels had a final concentration of MNPs of 0.0, 0.6 0.9, 1.7, 2.2 % by weight. Fig. 1(a) shows a general view of ferrogel samples with different concentrations of embedded MNPs in a geometry for GMI measurements. Fig. 1(b) shows a thin film sensitive element installed into the “microstripe line” sample holder with ferrogel slice (2 mm × 4 mm × 9 mm) prepared for measurements in the biosensor prototype regime.

2.2 Magnetoimpedance thin film sensitive element fabrication

The magnetic layers of the magnetoimpedance thin film sensitive element were $Fe_{19}Ni_{81}$ permalloy layers with close to zero magnetostriction. The multilayered elongated stripes (10 mm × 0.5 mm) were prepared by the sputtering technique and shaped by using metallic masks during deposition. Elements were deposited onto Corning glass substrates at room temperature with a background pressure of 3×10^{-7} mbar and a deposition argon pressure of 3.8×10^{-3} mbar. The deposition rates were 28 nm/min for FeNi and 25 nm/min for Cu layers. During the GMI stripe deposition, an external magnetic field of 100 Oe was applied along the short side of the GMI element in order to create a uniaxial magnetic anisotropy with low dispersion of the local anisotropy axes. Based on previous studies of MI structures with high sensitivity of magnetoimpedance responses with respect to external magnetic field [Kurlyandskaya, 2011; Scherbinin, 2017], the following multilayered structure was selected: [Cu (3 nm)/FeNi(100 nm)]$_5$/Cu(500 nm)/ [FeNi(100 nm)/Cu(3 nm)]$_5$. Fig. 1(c) shows the general scheme of the GMI multilayered structure.

2.3 Magnetic and magnetoimpedance measurements

Magneto-optical Kerr microscopy (MOKE) was used for the in-plane magnetic hysteresis loop measurements done for a full-sized sample: 10 mm × 0.5 mm. MOKE M(H) loops were measured from the free side of [Cu (3 nm)/FeNi(100 nm)]$_5$/Cu(500 nm)/[FeNi(100 nm)/Cu(3 nm)]$_5$ structure.

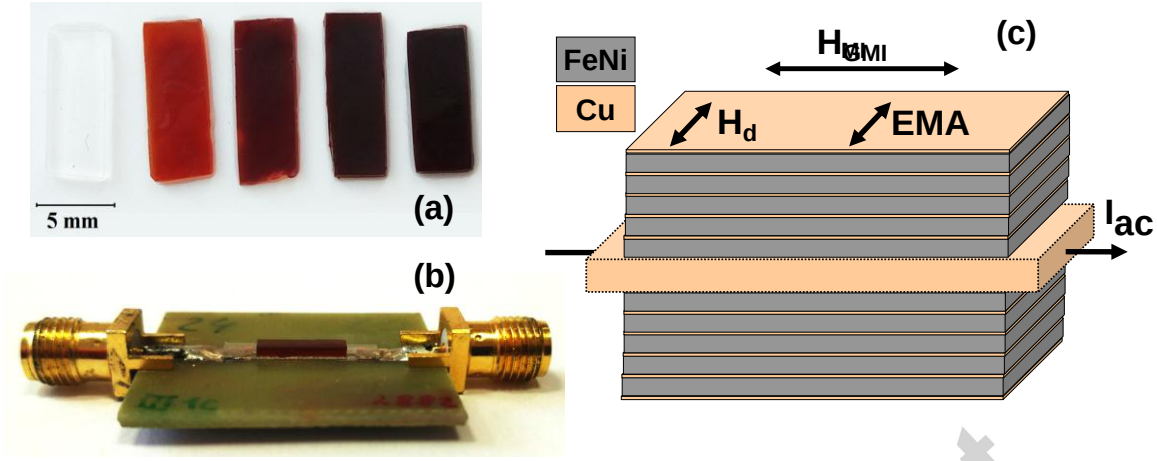

Fig. 1. General view of ferrogels with different concentrations of MNPs (from left to right 0.0, 0.6 0.9, 1.7, 2.2 wt. %) in a geometry for MI measurements (a). General view of MI "microstripe line" sample holder with ferrogel slice prepared for measurements in the biosensor prototype regime (b). Schematic representation of the MI multilayered structure: H_{MI} – orientation of the external magnetic field during GMI measurements; H_d- orientation of the technological external magnetic field applied during the deposition of the multilayered structure; EMA- easy magnetization axis formed during multilayer deposition and I_{ac} – intensity of the high frequency electric current, flowing in the direction of H_{MI} (c).

The hysteresis loops of gels and ferrogels were measured by Faraday vibrating sample magnetometer of laboratory design (VSM) for about 100 mg weight samples fixed in a polycarbonate capsule. In order to evaluate the capsule contribution, the hysteresis loop of a capsule was measured separately and carefully extracted from the M(H) data of the gel or ferrogel. All measurements were made at room temperature. The experimental error in the magnetization determination was within 1 %.

For MI measurements, a thin film multilayered element was incorporated into the "microstripe" line using silver paint (Figure 1(b)). A uniform external magnetic field was swept between +100 Oe and -100 Oe created by a pair of Helmholtz coils. An external field was applied along the long side of the GMI sensitive element, i.e. a longitudinal MI configuration for an alternating current flowing in the direction of the external magnetic field was used. The S_{11} reflection coefficient was measured by a network analyzer (Agilent E8358A) and the impedance changes were calculated on this basis. For all MI measurements corresponding to an output power of 0 dB, an excitation current across the multi-layered sample close to 1mA was used.

First, the direct current resistivity (R_{DC}) was measured for the GMI element installed on the "microstripe line". For MI measurements we used a previously established protocol of calibration and mathematical subtraction of the contributions corresponding to the test fixture [Fernandez, 2012]. Complex impedance (Z) was measured in a frequency range of 0.1- 100 MHz as a function of the applied magnetic field. The MI ratio for the prototype response was calculated as follows:

$$\frac{\Delta Z}{Z} = 100 \times \frac{Z(H) - Z(H_{\max})}{Z(H_{\max})} \qquad (1)$$

where H_{max} = 100 Oe. For the analysis of the changes of MI ratio with a frequency of alternating current the maximum value of the total impedance $(\Delta Z/Z)_{max}$ was also calculated. The experimental error in the impedance and impedance components determination was within 1 %.

3. Results and discussion

3.1. Characterization of nanoparticles, ferrogels and multilayered structures

Fig. 2(a) shows a TEM image of MNPs and a particle size distribution (PSD) histogram (inset). The particles are non-coalescent and their shape is very close to spherical. PSD is well fitted by a lognormal distribution function with a mean particle diameter of 17.3 nm and a lognormal dispersion of 0.413. The specific surface area of MNPs determined by low-temperature nitrogen adsorption (Micromeritics TriStar3000) was found to be as high as 64 m^2/g. The average surface diameter of MNPs, calculated from this value using the equation $d_s = 6/(\rho \times S_{sp})$ (ρ = 4.6 g/cm^3 being iron oxide density) was 20.7 nm. It was in fair agreement with the mean diameter of the PSD. The crystalline structure of MNPs according to the XRD (Bruker D8 Discover) corresponded to the inverse spinel lattice with a space group Fd3m, which is applicable both to magnetite (Fe_3O_4) and maghemite (γ-Fe_2O_3). The non-stoichiometric chemical composition of MNPs found by Red/Ox titration was $Fe_{2.73}O_4$, which is closer to maghemite.

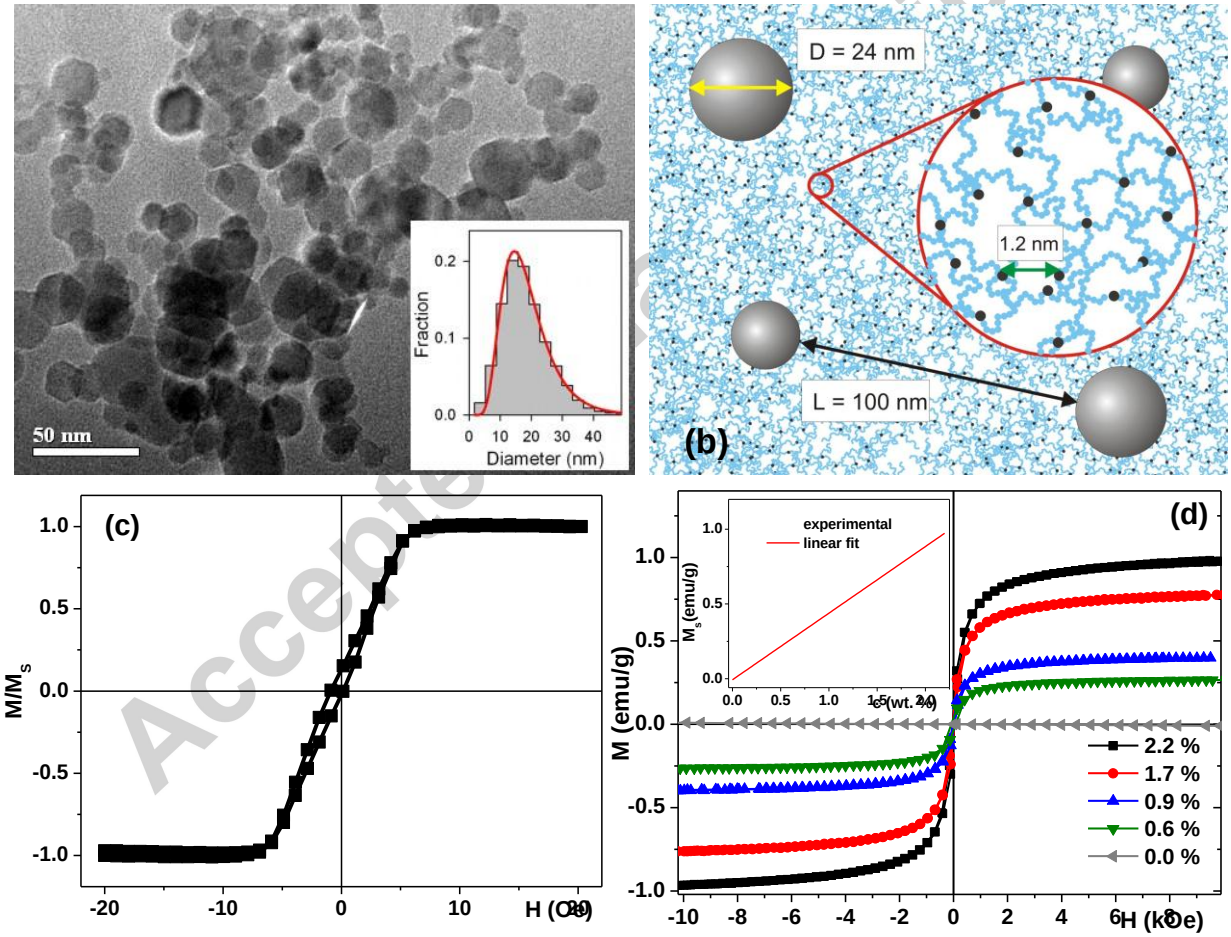

Fig. 2. TEM image of iron oxide MNPs embedded in ferrogels. Inset – particle size distribution (a). Graphical sketch of the internal ferrogel architecture (2.0 wt.% MNPs); inset – PAAm network, blue circles – monomer units in sub-chains, black circles – cross-links (b). MOKE M(H) hysteresis loop of MI multilayered rectangular element measured along the hard magnetization axis, i.e. the long side of the rectangle (c). M(H) hysteresis loops of ferrogels with different concentrations of MNPs (Inset showы the concentration dependence of magnetization of ferrogel samples in the field of 10 kOe) (c).

Fig. 2(b) presents the graphical sketch of the internal PAAm ferrogel architecture. The MNPs are embedded in an elastic polymeric network swollen in water. The network structure consists of entangled polymeric chains, which are randomly interconnected in multiple points by cross-links. The average distance between cross-links gives the apparent mesh size of its network and can be estimated based on the water uptake of the polymeric network (α). Using the thermogravimetry analysis (NETZSCH STA409), we established that the average distance was 7.0±0.4. Based on the value of α the average number of monomer units in linear sub-chains between cross-links (N_c) was evaluated using the Flory-Rehner equation [Quesada-Perez, 2011]:

$$N_C = \frac{V_1(0.5\alpha^{-1} - \alpha^{-1/3})}{V_2(\ln(1-\alpha^{-1}) + \alpha^{-1} + \chi\alpha^{-2})} \quad (2)$$

where V_1, V_2 – are molar volumes of a solvent and of a polymer respectively, χ – is the Flory-Huggins parameter for a polymer – solvent mixture. We used V_1=18 cm^3/mol (water), V_2= 56.2 cm^3/mol (PAAm) and χ= 0.12. The last two values were obtained by means of the quantum mechanics molecular modeling software package CAChe7.5. The obtained value Nc=16 means that there are 16 monomer units in PAAm subchains between adjacent cross-links on average. The length of the subchain can be evaluated as the mean square end-to-end distance of a random Gaussian coil with hindered rotation [Rubinstein, 2003]. Taken 0.154 nm for the length of the C–C bond and 109.5^o for the bond angle, the mesh size of the network was estimated at 1.2 nm. This value is by an order of magnitude smaller than the average diameter of the embedded iron oxide MNPs (24.4 nm). As a result, the MNPs can not freely move inside the polymeric network of the ferrogel but are entrapped in it. The average distance between MNPs in ferrogel can be easily estimated based on the concentration of MNPs. It gives around 100 nm between MNPs in the ferrogel with the highest content of iron oxide – 2.0 % (wt.) of them. The interparticle distance in other ferrogels was larger.

Polyelectrolyte gels consisting of a cross-linked network swollen in water are new materials which can be very useful for the development of magnetic biosensors. It is important to emphasize that the properties of the biomimetic gels and ferrogels, in contrast with the properties of biological tissues, can be set up during the synthesis and they can be thoroughly controlled in a physical experiment allowing repeatable tests. The flexible macromolecules contain polar residues, which provide the electric charge of the network compensated by simple counterions freely diffusible in a solution [Harland, 1992]. But the most important feature is the similarity of the molecular structure of the cell cytoskeleton immersed in a liquid and the 3D molecular structure of polyelectrolyte gels [Pullarkat, 2007]. A synthetic macromolecule and a protein consist of the same elements which provide the same types of molecular interactions showing a close similarity between the chemical composition and the supermolecular structure. Therefore, polyelectrolyte gels and ferrogels can substitute in certain studies true biological samples of natural tissues, which in turn allows to decrease the amount of animal testing.

Fig.2(c-d) summarizes the results of the magnetic measurements for thin films and ferrogels. The shape of the M(H) hysteresis loop of [Cu (3 nm)/FeNi(100 nm)]$_5$/Cu(500 nm)/[FeNi(100 nm)/Cu(3 nm)]$_5$ measured along the short size of the element confirms the formation of well-defined uniaxial induced magnetic anisotropy and the anisotropy field of about 7 Oe. In the case of ferrogels, full saturation was still not reached in the field of 10 kOe and we therefore used the magnetization value for H = 10 kOe as the saturation magnetization M_s just in order to check the Ms concentration dependence for the ferrogels (Inset Fig. 2(d)). The coercivity for all types of ferrogels was very small (below 10 Oe at room temperature) indicating that the majority of the MNPs were in a superparamagnetic state [J. M. D. Coey, 2010]. The non-zero value of the coercivity can be explained by the presence of a small fraction of large particles of the tail on the side of the large particle size distribution (inset Figure 2(a)). But generally speaking, we are

dealing with a superparamagnetic ensemble of iron oxide MNPs. One can also mention the low diamagnetic contribution of a gel matrix, which is practically negligible in comparison with the magnetic signals of MNPs of ferrogels.

3.2. MI response of multilayered structures: testing of biosensor prototype

Fig.3(a) shows the frequency dependence of the total impedance response of the GMI multilayered rectangular element itself (without gel or ferrogel). The shape of the GMI curve is typical for a multilayered sensitive element and it is in accordance with theoretical predictions [Kraus, 2003]. One can see that the highest value of the GMI ratio was observed near the 100 MHz frequency of the alternating current. In order to make the most justified selection of the working frequency for biosensor prototype testing we have recalculated the GMI sensitivity for the same frequency range (inset Fig.3(a)). MI sensitivity is understood as a change of the $\Delta Z/Z(H)$ ratio per unit value of the applied external magnetic field: $d(\Delta Z/Z)/dH$. The dashed rectangle shown in inset Fig.3(a) indicates the best frequency range for the biosensor prototype operation.

Fig.3(b) shows the field dependence of the total impedance response of the GMI multilayered rectangular element itself (without gel or ferrogel) measured from the highest value of the external field down to zero external field for the two selected frequencies. Inset Fig. 3(b) shows low field behavior of $\Delta Z/Z(H)$ responses. Both responses are close to each other and in both cases low field sensitivity (interval 1: 3.5 Oe < H < 6.0 Oe) and high field sensitivity (interval 2: 7.5 Oe < H < 9 Oe) intervals can be proposed for prototype testing.

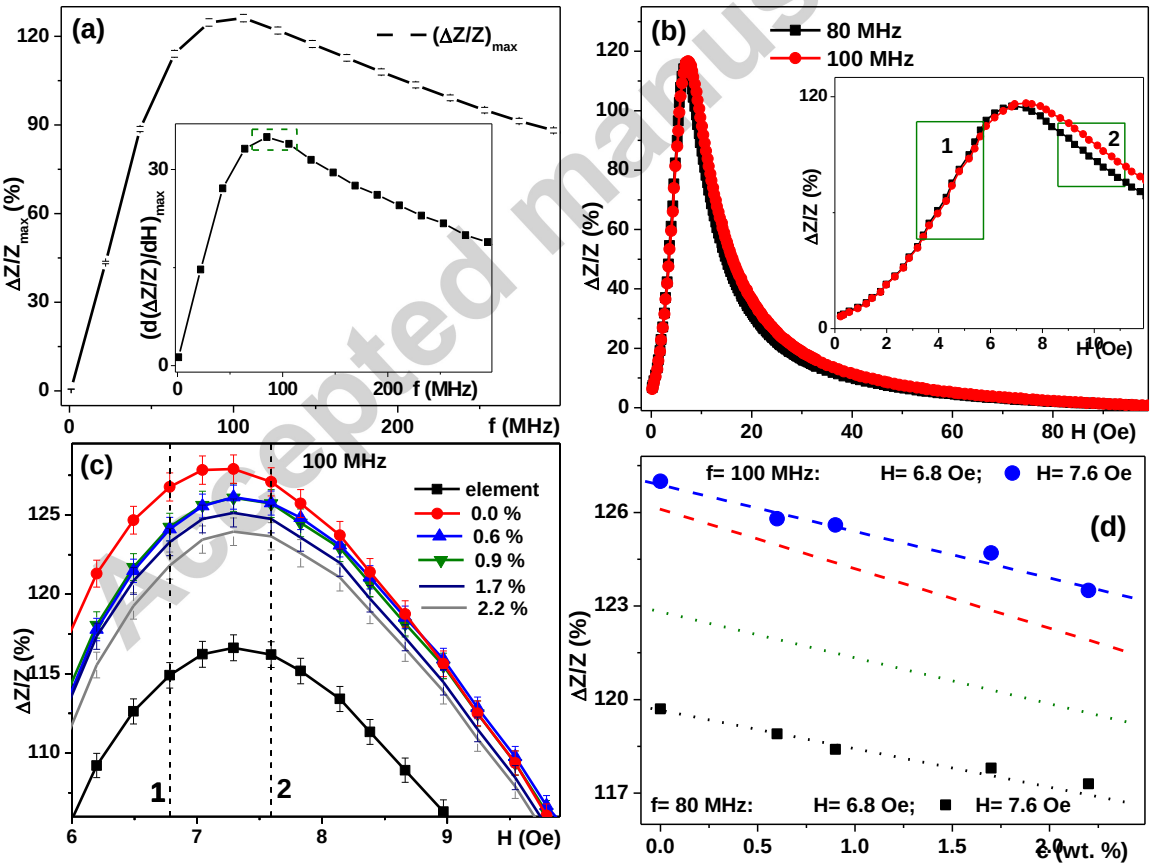

Fig. 3. Frequency dependence of the total impedance response of the [Cu (3 nm)/FeNi(100 nm)]$_5$/Cu(500 nm)/[FeNi(100 nm)/Cu(3 nm)]$_5$ rectangular element itself (without gel or ferrogel). Inset shows GMI sensitivity with respect to external field for the same frequency range

(a). Field dependence of the total impedance response of the [Cu (3 nm)/FeNi(100 nm)]$_5$/Cu(500 nm)/[FeNi(100 nm)/Cu(3 nm)]$_5$ element itself for selected frequencies (Inset: GMI responses near the anisotropy field with respect to external field for the same frequency range)(b). Field dependences of the total impedance responses of the GMI element in the presence of ferrogels with different concentrations of MNPs (c). Concentration dependences of the GMI ratio measured with the [Cu (3 nm)/FeNi(100 nm)]$_5$/Cu(500 nm)/[FeNi(100 nm)/Cu(3 nm)]$_5$ element for selected frequencies and selected external field values (d).

As the next step, the ΔZ/Z(H) responses were measured (see example of the experimental position in Fig. 1(a)) in the presence of the gel or ferrogel slice for either 80 or 100 MHz current frequency (Fig. 3(c)). Let us again select two particular field values: for 1 it is H = 6.6 Oe and for 2 it is H = 7.6 Oe. In the first case, this is a field below the anisotropy field and in the second case it is a field above the anisotropy filed. When the objective of the sensor design is simply to measure the external magnetic field value, the low field interval 1 is better as the field sensitivity there is d(ΔZ/Z)/dH= 36%/Oe. For the high field interval 2 the field sensitivity is much lower d(ΔZ/Z)/dH= 10 %/Oe. At the same time, conditions of the measurement of the stray fields created by MNPs embedded into the gel matrix are different in comparison to the simple measurement of the external magnetic field value. As the MNPs are close to a superparamagnetic state, for the creation of measureable stray fields they must be placed in the external magnetic field. Therefore, the high field interval 2 (Fig.3(b)) for the biosensor prototype functionality should be a compromise between the high sensitivity of the sensitive element with respect to the external field and the field in which stray field values are reasonably high. In fact, Fig. 3(d) confirms that both intervals (1 and 2) are very similar from the point of view of detection sensitivity: it was close to 1.3 % of ΔZ/Z per % of MNPs concentration by weight. Details of fit parameters used in Fig.3(d) are in Electronic Supplementary information (ESI).Both selected frequencies (of 80 and 100 MHz) insured almost the same sensitivity. In order to understand the obtained experimental results, we proposed and developed the following electromagnetic model.

3.3. MI response of multilayered structures: modelling of biosensor prototype with natural tissue mimicking samples

To describe the experimental results, we propose a model for the MI response of the multilayered film with the ferrogel layer. The influence of the ferrogel layer on the MI is related to stray fields induced by magnetic nanoparticles. The stray fields change the magnetization distribution in the magnetic layers of the film and affect the film permeability and MI effect. To describe qualitatively the influence of stray fields on the film MI, we assume that the ferrogel layer generates a spatially uniform effective field H_p in the film. The value of H_p is assumed to be proportional to the concentration of MNPs in the ferrogel, since the ferrogel saturation magnetization M_{sat} increases linearly (see Fig. 2(d)) with the concentration of nanoparticles. For simplicity, we present the field dependence of the ferrogel magnetization M_g by means of the linear function $M_g = M_{\text{sat}} \sin\varphi$, where the angle φ can be expressed as follows

$$\sin\varphi = (H - H_c)/(H_1 - H_c)\,. \qquad (3)$$

Here H_c is the coercivity of the ferrogel and H_1 is the value of the external field when $M_g = M_{\text{sat}}$.

It is assumed that the effective stray field H_p has the opposite direction with respect to the magnetization vector in the ferrogel layer. The magnetization distribution in the ferromagnetic layers of the film can be found by the free energy minimization leading to the following equation for the equilibrium magnetization angle θ:

$$H_a \sin(\theta-\psi)\cos(\theta-\psi) - H_p \sin(\theta-\varphi) - H\cos\theta = 0. \quad (4)$$

Here H_a is the anisotropy field in the ferromagnetic layers and ψ is the deviation angle of the anisotropy axis from the transverse direction.

The MI response of the film with the ferrogel layer can be found by means of a solution of Maxwell equations for the electromagnetic fields coupled with the Landau–Lifshitz equation for the magnetization dynamics. Since the film length *l* and width *w* are much higher than its thickness *t*, we can reduce the problem to a one-dimensional one and suppose that the electromagnetic fields depend only on the coordinate transverse to the film plane (*z*-coordinate).

In this approximation, the distribution of the longitudinal electric field and transverse magnetic field in the central layer and in the separating copper layers can be presented as follows:

$$\begin{aligned} e_1^{(j)} &= (c\lambda_0 / 4\pi\sigma_0)[A^{(j)}\cosh(\lambda_0 z) + B^{(j)}\sinh(\lambda_0 z)], \\ h_1^{(j)} &= A^{(j)}\sinh(\lambda_0 z) + B^{(j)}\cosh(\lambda_0 z) \end{aligned} \quad (5)$$

Here $e_1^{(j)}$ and $h_1^{(j)}$ are the amplitudes of the electric and magnetic field, $j = 1,\ldots,11$ is the copper layer number, $A^{(j)}$ and $B^{(j)}$ are the constants, $\lambda_0 = (1-i)/\delta_0$, $\delta_0 = c/(4\pi^2 f\sigma_0)^{1/2}$, f is the frequency, σ_0 is the copper conductivity, and *c* is the velocity of light.

The field amplitudes $e_2^{(k)}$ and $h_2^{(k)}$ in the permalloy layers can be expressed as

$$\begin{aligned} e_2^{(k)} &= (c\lambda_m / 4\pi\sigma_m)[C^{(k)}\cosh(\lambda_m z) + D^{(k)}\sinh(\lambda_m z)], \\ h_2^{(k)} &= C^{(k)}\sinh(\lambda_m z) + D^{(k)}\cosh(\lambda_m z) \end{aligned} \quad (6)$$

Here $k = 1,\ldots,10$ is the permalloy layer number, $C^{(k)}$ and $D^{(k)}$ are the constants, $\lambda_m = (1-i)/\delta_m$, $\delta_m = c/(4\pi^2 f\mu\sigma_m)^{1/2}$, σ_m and μ are the conductivity and transverse permeability of the permalloy layers, respectively.

Since in the experiment the current frequencies are sufficiently high, the value of the transverse permeability μ in the ferromagnetic layers is governed by the magnetization rotation. The solution of the linearized Landau–Lifshitz equation results in the following expression for the transverse permeability [Panina, 1995]:

$$\mu = 1 + \frac{\omega_m[\omega_m + \omega_1 - i\kappa\omega]\sin^2\theta}{[\omega_m + \omega_1 - i\kappa\omega][\omega_1 - \gamma H_a \sin^2(\theta-\psi) - i\kappa\omega] - \omega^2}. \quad (7)$$

Here $\omega_m = 4\pi\gamma M$, M is the saturation magnetization of the permalloy layers, γ is the gyromagnetic constant, κ is the Gilbert damping parameter, $\omega = 2\pi f$ is the angular frequency, the equilibrium magnetization angle θ is given by Eq. (4) and

$$\omega_1 = \gamma[H_a\cos^2(\theta-\psi) - H_p\cos(\theta-\varphi) + H\sin\theta] \quad (8)$$

The solution of Maxwell equations in the ferrogel layer can be presented in the form

$$\begin{aligned} e_3 &= [E\cosh(\lambda_g z) + F\sinh(\lambda_g z)]/\varepsilon^{1/2}, \\ h_3 &= E\sinh(\lambda_g z) + F\cosh(\lambda_g z) \end{aligned} \quad (9)$$

Here e_3 and h_3 are the amplitudes of the electric and magnetic field in the ferrogel, E and F are the constants, ε is the permittivity of the ferrogel and $\lambda_g = -i\omega\varepsilon^{1/2}/c$.

To describe the field distribution in the external regions we use the approximate solution for the vector potential obtained previously for $t << w$ [Gromov, 1999; Sukstanskii, 2001]. The field amplitudes are given by

$$e_m = G_m \frac{i\omega}{c}\left[\frac{l}{2w}\log\left(\frac{R+w}{R-w}\right) - \frac{2z}{w}\arctan\left(\frac{wl}{2Rz}\right) + \frac{1}{2}\log\left(\frac{R+l}{R-l}\right)\right],$$
$$h_m = -G_m \frac{4lz}{R}\left[\frac{R^2+4z^2}{4R^2z^2+l^2w^2} - \frac{1}{R^2-w^2} - \frac{1}{R^2-l^2}\right] + G_m \frac{2}{w}\arctan\left(\frac{wl}{2Rz}\right). \quad (10)$$

Here subscripts $m = 4$ and $m = 5$ correspond to the bottom and top external region, respectively, G_m are the constants and $R = (l^2 + w^2 + 4z^2)^{1/2}$.

The constants in Eqs. (5), (6), (9) and (10) can be found from the continuity conditions for the amplitudes of the electric and magnetic fields at the interfaces between different regions allowing one to describe completely the distribution of the electromagnetic fields. Taking into account that the driving electric field with the amplitude e_0 is applied to the film structure only, we can find the impedance Z of the film with ferrogel layer as a ratio of the applied voltage to the total current flowing through the film

$$Z = \frac{le_0}{w\int_{-t/2}^{t/2}\sigma(z)e(z)\mathrm{d}z} \quad (11)$$

Fig. 4(a) shows the field dependence of the MI ratio $\Delta Z/Z$ calculated at 100 MHz for the film without ferrogel and the film with ferrogel for different values of the effective stray field H_p. Note that the results are presented only for the range of positive fields, since the MI ratio is symmetric with respect to the sign of the external field. In the presence of the gel without MNPs ($H_p = 0$), the MI ratio increases due to the high the permittivity of the gel. The effective stray field increases with the concentration of MNPs in the ferrogel due to the growth of the ferrogel saturation magnetization. As a result, the MI ratio decreases with an increase of H_p (see Fig. 4(a)) exhibiting a dependence similar to the one observed in the experiment.

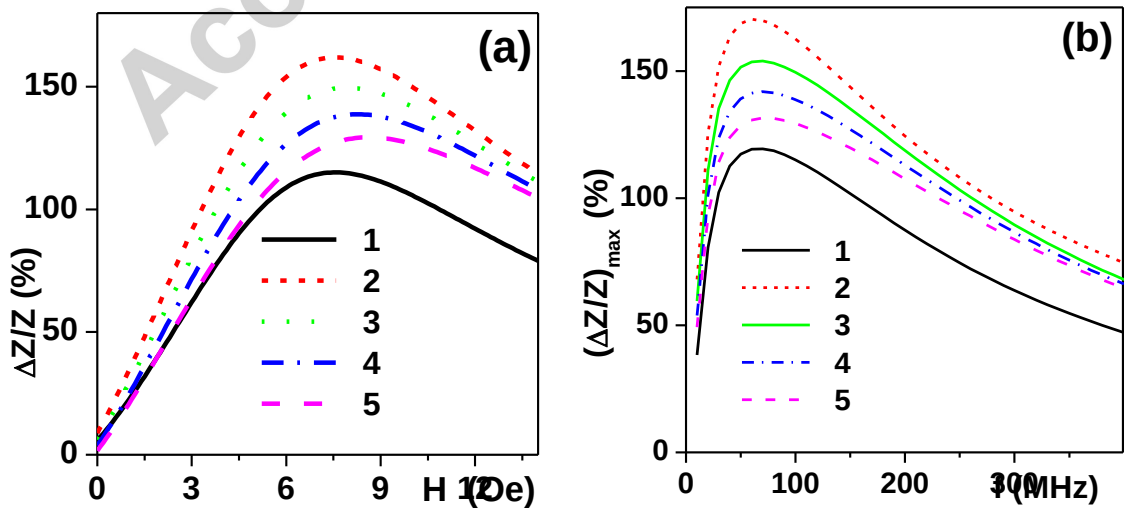

Fig. 4. Calculated MI ratio as a function of the external field at $f = 100$ MHz (a) and frequency dependence of the maximum value of MI ratio (b). Curves 1, film without gel; curves 2, $H_p = 0$; curves 3, $H_p = 0.25$ Oe; curves 4, $H_p = 0.5$ Oe; curves 5, $H_p = 0.75$ Oe. Parameters used for calculations are $M = 750$ G, $H_a = 6$ Oe, $\psi = -0.1\pi$, $\sigma_0 = 5 \times 10^{17}$ s^{-1}, $\sigma_m = 3 \times 10^{16}$ s^{-1}, $\kappa = 0.02$, $H_c = 6.5$ Oe, $H_1 = 750$ Oe and $\varepsilon = 70$.

The calculated frequency dependence of the maximum value of MI ratio $\Delta(Z/Z)_{\max}$ is presented in Fig. 4(b). The dependence is in a qualitative agreement with experimental results. However, the model predicts that the maximum value of $\Delta(Z/Z)_{\max}$ appears at the lower frequency of about 80 MHz. The disagreement between the experimental and calculated results may be attributed to approximations in the proposed model.

3.5. MI response of multilayered structures: comparison of experimental and modelling results

It should be mentioned specially that the gel presence resulted in a large increase of $(\Delta Z/Z)_{\max}$ ratio for the given frequency in a wide frequency range. Such an increase was also obtained in the model calculations. The large change of MI response in the presence of gel the sample indicates a high capacity of magnetoimpedance spectroscopy to be a useful technique for the evaluation of the properties of natural gels even in the absence of embedded MNPs. This might be a new direction in magnetic biosensing. The MI response in the presence of the ferrogel is conditioned by the presence of at least two contributions causing a different behavior. The gel matrix due to the high dielectric constant of the gel leads to the increase of the $\Delta Z/Z$ ratio but an increase of the MNPs concentration in the gel results in a decrease of the $\Delta Z/Z$ value.

In our previous works related to magnetic biosensing using an MI sensor prototype, the origin of sensitivity to the stray fields of magnetic particles was not mathematically described and analysed. In the work (Kurlyandskaya, 2003) the sensitive element was a rapidly quenched amorphous ribbon: a good choice but the option was less compatible with present day semiconductor electronics in comparison with a thin film sensitive element. It was a close-proximity sensor for in-vitro geometry in which all MNPs had to be situated at very short distances from the surface. In the work (Kurlyandskaya, 2015) we presented a phenomenological result for measurements of gel/ferrogel samples without any theory and had experimentally measured the concentration dependence for the MNPs embedded in the gel matrix using very large samples of the order of 1 g mass. In the present study, specially designed to be able to compare theoretical calculations and experimental results, the mass of the testing sample was one order of magnitude smaller.

We have made the next step towards the development of a biosensor for in-tissue embedded magnetic nanoparticle detection for the case uniform ferrogels mimicking natural tissue. To make this promising technique useful for practical applications of magnetically labeled tissue detection, a synthesis of composite gels with MNP agglomerates compactly located inside pure gel and their MI testing are necessary. In addition, we should mention that gels/ferrogels are very promising materials for regenerative medicine and drug delivery applications [Harris, 2011; Blyakhman, 2017], but up to now they were synthesized as uniform structural units. In this sense they are less useful for mimicking cancer tissue with huge variations of the structural morphologies [Grossman, 2012] or materials for drug loading.

Conclusion

In summary, in order to mimic natural tissue with embedded MNPs we synthesized chemically crosslinked hydrogels filled with maghemite γ-Fe_2O_3 MNPs. [Cu

/FeNi]$_5$/Cu/[FeNi/Cu]$_5$ rectangular elements were designed and tested. Magnetoimpedance sensor prototype responses were measured with and without polyacrylamide ferrogel layer in order to evaluate stray fields of MNPs. A corresponding MI model was developed on the basis of the solution of linearized Maxwell equations and Landau-Lifshitz equation for the magnetization dynamics in order to understand the origin of the prototype sensitivity which reached 1.3 % of $\Delta Z/Z$ per % of MNPs concentration by weight. One of the directions of the future work will be the development of ferrogels with controlled porosity for regenerative medicine and drug delivery. In this field the magnetic detector which is described in the present work can be an extremely useful instrument for gel/ferrogel characterization.

Acknowledgement

This work was supported by the RSF grant 18-19-00090. We thank I.V. Beketov, S.O. Volchkov, G.Yu. Melnikov, A. Larrañaga and A.A. Gallet for special support.

References

Baselt, D.R., Lee, G.U., Natesan, M., Metzger, S.W., Sheehan, P.E.; Colton, R.J., 1998. Biosens. Bioelectron. 13, 731–739.

Beketov, I.V., Safronov, A.P., Medvedev, A. I., Alonso, J., Kurlyandskaya, G.V., Bhagat, S.M., 2012, AIP Advances 2, 022154.

Besse, P.-A., Boero, G., Demierre, M., Pott, V., Popovic, R., 2002. Appl. Phys. Lett. 80, 4199–4201.

Blanc-Beguin, F., Nabily, S., Gieraltowski, J., Turzo, A., Querellou, S., Salaun, P.Y., 2009. J. Magn. Magn. Mater. 321, 192–197.

Blyakhman, F.A., Safronov A.P., Zubarev A.Yu., Shklyar T.F., Makeyev O.G., Makarova, E.B., Melekhin V.M., Larrañaga, A, Kurlyandskaya, G.V., 2017. Results in Physics 7, 3624–3633.

Chen, Zh., Wu, Y., Kang, M., He, N., Wan, S., Su, E., Wang, L., 2018. Nanosci. Nanotechnol. Lett. 10, 60-68.

Chung, S. J., Leonard, J. P., Nettleship, I., Lee, J. K., Soong, Y., Martello, D. V., Chyu, M. K. 2009. Powder Technology 194, 75-80.

Coey, J.M.D., 2010. Magnetism and Magnetic Materials. Cambridge University Press, New York, USA..

Devkota, J., Trang, M.T., Stojak, K., Ha, P.T., Pham, H.N., Nguyen, X.P., Mukherjee, P., Srikanth, H., Phan, M.H., 2014. Sens. Actuators B 190, 715-722.

Gromov, A., Korenivski, V., Haviland, D., van Dover, R.B., 1999. J. Appl. Phys. 85, 5202-5204.

Harris R., Lecumberri, E., Mateos-Aparicio I., Mengíbar, M., Heras, A., 2011. Carbohydrate Polymers 84, 803-806.

Hwang, Y., Lee, J.-K., Jeong, Y.-M., Cheong, S., Ahn, Y.-Ch., Kim, S.H., 2008. Powder Technology 186, 145-153.

García-Arribas, A., Martínez, F., Fernández, E., Ozaeta, I., Kurlyandskaya, G.V., Svalov, A.V., Barandiaran, J.M., 2011. Sens. Actuators A 172, 103-108.

Graham, D.L., Ferreira, H.A., Freitas, P.P., Cabral, J.M.S., 2003. Biosens. Bioelectron. 18, 483-488.

Grossman, J.H., McNeil, S.E., 2012. Phys. Today 65, 38–42.

Glaser, R., 1999. Biophysics. Springer Verlag, Heidelberg, Germany.

Fernandez, E., Svalov, A.V., García-Arribas, A., Feuchtwanger, J., Barandiaran, J.M., Kurlyandskaya, G.V., 2012. J. Nanosci. Nanotechnol. 12, 7496–7500.

Ferreira, H.A., Graham, D.L., Freitas, P.P., Cabral, J.M.S., 2002. J. Appl. Phys. 93, 7281–7286.

Harland, R.S., Prudhomme, R.K., 1992. Polyelectrolyte gels: properties, preparation and applications, American Chemical Society, Washington, DC, USA.

Huang, S., Yang, H., Lakshmanan, R.S., Johnson, M.L., Wan, J., Chen, I.H., Wikle, H.C., Petrenko, V.A., Barbaree, J.M.; Chin, B.A., 2009. Biosens. Bioelectron. 24, 1730–1736.

Kraus, L., 2003. Sens. Actuators A 106, 187-194.

Kurlyandskaya, G.V., Sánchez, M.L., Hernando, B., Prida, V.M., Gorria, P., Tejedor, M., 2003. Appl. Phys. Lett. 82, 3053-3056.

Kurlyandskaya, G., Levit, V., 2005. Bios. Bioelectr. 20, 611-616.

Kurlyandskaya, G.V., Fal Miyar V., 2007. Biosens. Bioelectron. 22, 2341–2345.

Kurlyandskaya, G.V., Garcia-Arribas, A., Fernandez, E., Svalov, A.V., 2012. IEEE Trans. Magn. 48, 1375–1380.

Kurlyandskaya, G.V., Fernandez, E., Safronov, A.P., Svalov, A.V., Beketov, I.V., Burgoa Beitia, A., Garcıa-Arribas, A., Blyakhman, F.A., 2015. Appl. Phys. Lett. 106, 193702.

Kurlyandskaya, G.V., Novoselova, Iu.P., Schupletsova, V.V., Andrade, R., Dunec, N.A., Litvinova, L.S., Safronov, A.P., Yurova, K.A., Kulesh, N.A., Dzyuman, A.N., Khlusov, I.A., 2017. J. Magn. Magn. Mater. 431, 249–254.
Landau, L.D., Lifshitz, E.M.. 1975. Electrodynamics of Continuous Media; Pergamon: New York, NY, USA.
Lopes, A.C., Sagasti, A., Lasheras, A., Muto, V., Gutiérrez, J., Kouzoudis D., Barandiarán, J.M., 2018. Sensors 18, 887.
Makhotkin, V.E., Shurukhin, B.P., Lopatin, V.A., Marchukov, P.Y., Levin, Y.K., 1991. Sens. Act. A 27, 759–762.
Miller, M.M., Prinz, G.A., Cheng, S.-F., Bounnak, S., 2002. Appl. Phys. Lett. 81, 2211–2213.
Ong, K.G., Wang, J., Singh, R.S., Bachas, L.G., Grimes, C.A., 2001. Biosens. Bioelectron. 16, 305.
Osipov, V.V., Platonov, V.V., Uimin, M.A., Podkin, A.V., 2012. Tech. Phys. 57, 543–549.
Quesada-Perez, M., Maroto-Centeno, J.A., Forcada, J., Hidalgo-Alvarez, R., 2011. Soft Matter. 7, 10536-10547.
Pacek, A. W., Ding, P., Utomo, A. T., 2007. Powder Technology 173, 203-2010.
Panina, L.V. Mohri, K., Ushiyama, T., Noda, M., Bushida, K., 1995. IEEE Trans. Magn. 31, 1249-1260.
Pullarkat, P.A. Fernandez, P.A. Ott, A. 2007. Phys. Rep. 449, 29-53.
M. Rubinstein, R.H. Colby. Polymer physics. New York: Oxford University Press. 2003. p. 59.
Rusakov, V., Raikher, Yu., 2018. Sensors 18, 1661.
Safronov, A.P., Mikhnevich, E.A., Lotfollahi, Z., Blyakhman, F.A., Sklyar, T.F., Larrañaga, A., Medvedev, A.I., Fernández Armas, S., Kurlyandskaya, G.V., 2018. Sensors 18, 257.
Shanmugam, S., Nakanishi, T. Osaka, T., 2009. ECS Trans. 16, 189–197.
Shcherbinin, S.V., Volchkov, S.O., Lepalovskii, V.N., Chlenova, A.A., Kurlyandskaya, G.V., 2017. Russ. J. Nondestr. Test. 53, 204–212.
Sukstanskii, A., Korenivski, V., Gromov, A., 2001. J. Appl. Phys. 89, 775-782.
Wang, T., Zhou, Y., Lei, Ch., Luo, J., Xie, Sh., Pu, H., 2017. Biosens. Bioelectr. 90, 418-435.
Uchiyama, T., Mohri, K., Honkura, Y., Panina, L.V., 2012. IEEE Trans. Magn. 48, 3833–3839.
Wong, J., Chilkoti, A., Moy, V.T., 1999. Biomol. Eng. 16, 45–55.
Yang, H., Chen, L., Lei, C., Zhang, J., Li, D., Zhou, Z.-M., Bao, C.-C., Hu, H.-Y., Chen, X., Cui, F., Zhang, S.-X., Zhou, Y., Cui, D.-X., 2010. Appl. Phys. Lett. 97, 043702.
Zhang, Y., Chen, Y., Westerhoff, P., Hristovski, K., Crittenden, J. C., 2008. Water Res. 42, 2204.

Highlights

- Magnetoimpedance (MI) biosensior prototype with $[Cu/FeNi]_5/Cu/[FeNi/Cu]_5$ element was designed and tested.
- MI responses were measured with and without ferrogel layer mimicking natural tissue.
- We were able to evaluate stray fields of 3D distributions of embedded magnetic nanoparticles.
- Electromagnetic MI model was developed in order to understand the 1.3 % of $\Delta Z/Z$ per 1 wt. % of MNPs concentration prototype sensitivity.